Article

Cell Reports

Routing Hippocampal Information Flow through Parvalbumin Interneuron Plasticity in Area CA2

Graphical Abstract

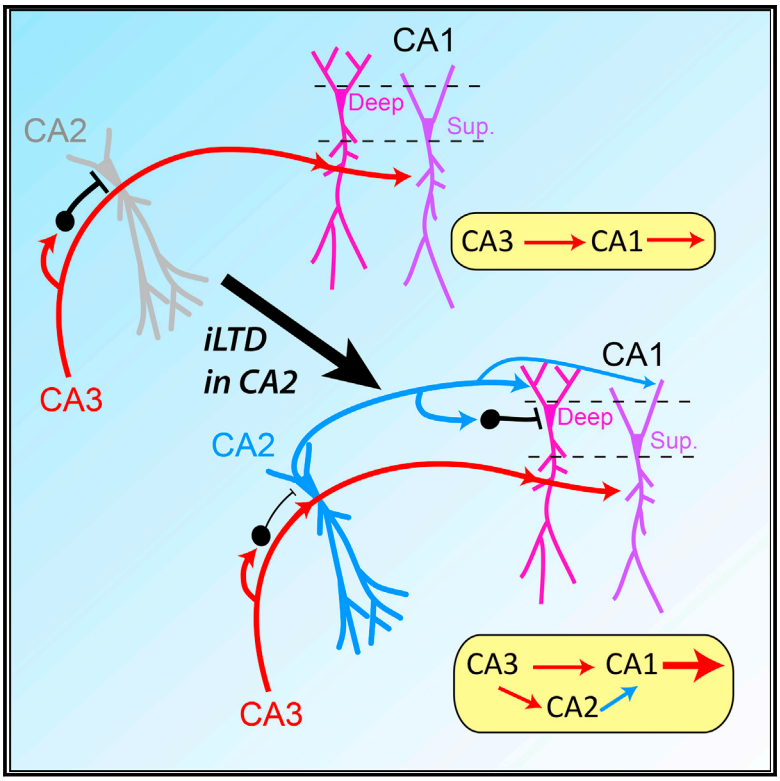

Highlights

- Parvalbumin-expressing interneurons control the recruitment of CA2 by CA3 input
- Feed-forward inhibition normalizes excitation from CA2 onto deep and superficial CA1
- CA2 inputs strongly excite radiatum giant cells in area CA1
- Recruitment of CA2 by CA3 substantially increases CA1 output

Authors

Kaoutsar Nasrallah, Ludivine Therreau, Vincent Robert, Arthur J.Y. Huang, Thomas J. McHugh, Rebecca A. Piskorowski, Vivien Chevaleyre

Correspondence

rebecca.piskorowski@parisdescartes.fr (R.A.P.), vivien.chevaleyre@parisdescartes.fr (V.C.)

In Brief

Nasrallah et al. show how recruitment of CA2 pyramidal neurons can considerably influence CA1 output when these cells are recruited by CA3. Parvalbumin-expressing interneurons have a critical role in regulating CA2 output and normalize the excitatory drive from CA2 to CA1. In addition, CA2 strongly excites radiatum giant cells.

Nasrallah et al., 2019, Cell Reports *27*, 86–98
April 2, 2019 © 2019 The Author(s).
https://doi.org/10.1016/j.celrep.2019.03.014

CellPress

OPEN ACCESS
CellPress

Cell Reports
Article

Routing Hippocampal Information Flow through Parvalbumin Interneuron Plasticity in Area CA2

Kaoutsar Nasrallah,[1,3] Ludivine Therreau,[1] Vincent Robert,[1] Arthur J.Y. Huang,[2] Thomas J. McHugh,[2] Rebecca A. Piskorowski,[1,*] and Vivien Chevaleyre[1,4,*]

[1]Team Synaptic Plasticity and Neural Networks, INSERM UMR-S1266 Institute of Psychiatry and Neuroscience of Paris, Université Paris Descartes, 102-108 Rue de la Santé, 75014 Paris, France

[2]Laboratory for Circuit and Behavioral Physiology, RIKEN Center for Brain Science, 2-1 Hirosawa, Wakoshi, Saitama 351-0198, Japan

[3]Present address: Dominick P. Purpura Department of Neuroscience, Albert Einstein College of Medicine, Bronx, NY 10461, USA

[4]Lead Contact

*Correspondence: rebecca.piskorowski@parisdescartes.fr (R.A.P.), vivien.chevaleyre@parisdescartes.fr (V.C.)

https://doi.org/10.1016/j.celrep.2019.03.014

SUMMARY

The hippocampus is critical for the formation of episodic memory. It is, therefore, important to understand intra-hippocampal circuitry, especially in the often overlooked area CA2. Using specific transgenic mouse lines combined with opto- and chemogenetics, we show that local plasticity of parvalbumin-expressing interneurons in area CA2 allows CA3 input to recruit CA2 pyramidal neurons (PNs), thereby increasing the excitatory drive between CA3 and CA1. CA2 PNs provide both stronger excitation and larger feed-forward inhibition onto deep, compared with superficial, CA1 PNs. This feed-forward inhibition, largely mediated by parvalbumin-expressing interneurons, normalizes the excitatory drive onto deep and superficial CA1 PNs. Finally, we identify a target of CA2 in area CA1, i.e., CA1 PNs, whose soma are located in *stratum radiatum*. These data provide insight into local hippocampal circuitry and reveal how localized plasticity can potentially control information flow in the larger hippocampal network.

INTRODUCTION

Hippocampal area CA2 has recently emerged as an important region for hippocampal activity and hippocampal-dependent memory. In particular, activity in area CA2 was shown to be critical for aggressive behavior (Pagani et al., 2015) and the formation of social memory (Hitti and Siegelbaum, 2014; Stevenson and Caldwell, 2014). It could also contribute to contextual memory (Wintzer et al., 2014) and potential temporal coding (Mankin et al., 2015). How this small region contributes to these functions remains to be understood. Recordings of CA2 pyramidal neuron (PN) activity during spatial exploration have revealed that cells in this region display activity that contrasts to that of areas CA1 and CA3. Specifically, area CA2 was shown to be an initiation zone for sharp-wave ripples (Oliva et al., 2016), a network-wide oscillation that has a major role in memory consolidation (Buzsáki, 2015). Furthermore, it has been shown that a subset of PNs in area CA2 encode spatial information during immobility (Kay et al., 2016). Thus, given this recent evidence, a better understanding of the local network controlling CA2 activity and connection to area CA1 is required to better understand how this region acts on hippocampal network activity and memory formation.

Excitation of CA3 Schaffer collaterals drives a very large feed-forward inhibition in area CA2 (Chevaleyre and Siegelbaum, 2010). Consistent with the higher density of interneurons compared with other hippocampal areas (Botcher et al., 2014; Piskorowski and Chevaleyre, 2013), inhibition prevents CA3 neurons from engaging CA2 PNs. In contrast to CA3 excitatory inputs that do not express activity-dependent plasticity (Zhao et al., 2007), this feed-forward inhibitory transmission in area CA2 expresses a unique long-term depression (iLTD) mediated by activation of delta opioid receptors (DOR) (Piskorowski and Chevaleyre, 2013). After iLTD induction, CA3 inputs are able to drive action potential firing in CA2 PNs (Nasrallah et al., 2015). The consequences of the recruitment of CA2 by CA3 on area CA1 activity after iLTD are unexplored.

We predict that recruitment of CA2 by CA3 activity will have consequences on area CA1, the main hippocampal output. CA2 PNs have been shown to mediate a direct excitation onto CA1 PNs (Chevaleyre and Siegelbaum, 2010). Interestingly, CA2 PNs were shown to make a stronger excitatory connection onto deep CA1 PNs, i.e., those closer to *stratum oriens*, as compared with superficial CA1 PNs, i.e., those closer to *stratum radiatum* (Kohara et al., 2014). This is of relevance because deep CA1 PNs in the ventral hippocampus have recently been shown to encode social information (Okuyama et al., 2016). It has been shown that CA2 PNs also recruit feed-forward inhibition in area CA1 (Valero et al., 2015). However, the effect of this inhibition on the direct excitation between CA2 and CA1 PNs is not known. Furthermore, it was shown that the CA2-CA3 connection is dominated by a large feed-forward inhibition that tightly controls the recruitment of CA3 PNs by the dentate gyrus (Boehringer et al., 2017). This inhibition controls the timing of CA3 action potential firing, and removal of CA2 input by expression of tetanus toxin light chain in CA2 pyramidal neurons resulted in

This is an open access article under the CC BY-NC-ND license (http://creativecommons.org/licenses/by-nc-nd/4.0/).

hypersynchrony of CA3 firing and the emergence of large synchronous events that propagated to area CA1 (Boehringer et al., 2017).

In this study, we used chemogenetics, optogenetics, and electrophysiology to examine how the recruitment of CA2 PNs by CA3 activity after inhibitory plasticity translates onto the excitatory drive of different populations of CA1 PNs. We found that parvalbumin-expressing (PV^+) interneurons underlie iLTD in area CA2 and the decreased transmission from PV^+ cells is sufficient to allow CA3 input to recruit CA2 PNs. We further found that the recruitment of CA2 PNs after iLTD induction strongly increases the excitatory drive between CA3 and CA1 PNs. This extra-synaptic drive from CA2 to CA1 is tightly controlled by feed-forward inhibition from PV^+ interneurons and acts to normalize the excitatory drive onto deep and superficial CA1 PNs. Finally, we report that CA2 PNs strongly project to radiatum giant cells, PNs in area CA1 with soma located in the *stratum radiatum*.

RESULTS

PV^+ Interneurons Mediate the DOR-Dependent Dis-inhibitory Plasticity in CA2

In the hippocampus, DORs are mostly expressed by PV^+ interneurons (Erbs et al., 2012), and area CA2 contains a high density of this subclass of interneurons (Botcher et al., 2014; Piskorowski and Chevaleyre, 2013). Stimulation of CA3 Schaffer collateral inputs recruits a large feed-forward inhibition in area CA2 (Chevaleyre and Siegelbaum, 2010) that undergoes an iLTD mediated by DOR activation (Piskorowski and Chevaleyre, 2013) and allows a dis-inhibitory increase in CA3-CA2 transmission (Nasrallah et al., 2015). Thus, we predicted that the DOR-dependent dis-inhibitory increase in CA3-CA2 transmission would be mediated by a decrease in GABA release from PV^+ cells. To test whether PV^+ interneurons are necessary and sufficient for this plasticity, we bilaterally injected a cre-recombinase-dependent adeno-associated virus (AAV) vector expressing an inhibitory designer receptor exclusively activated by a designer drug (Gi-DREADD-mcherry) into the hippocampi of 6- to 8-week-old Pvalb-cre transgenic mice. Thus, in acute slices that were prepared 6 weeks later, we were able to inhibit synaptic transmission selectively from PV^+ interneurons with the bath application of the DREADD agonist clozapine N-oxide (CNO). Using immunohistochemistry, we first verified that the Gi-DREADD-mcherry expression was selective for PV^+ interneurons (Figures 1A and 1B). We found that 96.3% ± 1.6% of cells expressing Gi-DREADD-mCherry were also positive for parvalbumin (PV). Conversely, 67.4% ± 3.5% of PV^+ cells also expressed mCherry. Therefore, the Gi-DREADD is indeed expressed in most PV^+ interneurons but not by other interneuron populations. We then asked whether silencing PV^+ interneurons would be sufficient to control the strength of excitatory transmission between CA3 and CA2. We performed whole-cell current-clamp recordings of CA2 PNs and monitored the amplitude of the post-synaptic potentials (PSPs) in response to CA3 input stimulation. These PSPs consist of compound excitatory and inhibitory post-synaptic potentials. We found that application of CNO (10 μM) induced a large increase in the depolarizing phase of the PSP amplitude (Figure 1C; 203.0% ± 25.5% of baseline, n = 9, p = 0.003). Next, because feed-forward inhibitory transmission between CA3 and CA2 prevents CA3 inputs to engage CA2 PNs, we wondered whether silencing PV^+ interneurons could also increase action potential (AP) firing in CA2. To prevent dialysis of the recorded cell and avoid altering intrinsic properties of the PNs, we performed extracellular recordings in the somatic layer of area CA2 to measure a population spike (PS) in response to CA3 input stimulation before and after CNO application. In agreement with previous studies (Chevaleyre and Siegelbaum, 2010; Nasrallah et al., 2015), we found that the PS amplitude was very small or not detectable in basal conditions, even at the highest stimulation intensity (Figure 1D). Interestingly, application of CNO induced the emergence of a PS for all stimulation intensities (Figure 1D; for instance, from 0.029 ± 0.002 mV to 0.070 ± 0.008 mV, p = 0.0019 at 20 V stimulation, n = 6). Decreasing inhibitory transmission from approximately two-thirds of PV^+ INs, as was done with Gi-DREADD, might be too strong of a manipulation in comparison with the decrease in PV transmission that occurs with DOR-mediated iLTD. Thus, we wondered what fraction of feed-forward inhibition is reduced by CNO application and whether a more moderate decrease in PV^+ IN transmission could also reveal AP firing in CA2 PNs. First, we determined the effect of CNO on inhibitory post-synaptic current (IPSC) amplitude at +10 mV (around the reversal potential for excitatory transmission) with excitation unblocked to include feed-forward inhibition. We found that CNO reduced inhibitory transmission by ~35% (Figure S1A; 65.2% ± 1.6% of baseline, n = 5; p = 0.000065). Using slices prepared from 6- to 8-week-old mice, we used the DOR agonist [D-Pen^2,D-Pen^5]enkephalin (DPDPE; 5 μM) to depress a smaller fraction of PV^+ INs and tested whether this manipulation would be sufficient to reveal AP firing in CA2 PNs. DORs are primarily expressed by a subpopulation of PV^+ INs, representing ~35% of all PV^+ INs (Erbs et al., 2012). We used cell-attached recording to prevent altering the excitability of PNs. We observed no AP before DPDPE application in response to CA3 input stimulation. However, application of DPDPE revealed the appearance of APs in ~80% of the cells, thus leading to a significant increase in AP probability (Figure S1B; at 30 V, AP probability during first stimulation, 0.36 ± 0.10, p = 0.0065; AP probability during second stimulation, 0.53 ± 0.10, p = 6.2 × 10^{-4}, n = 10). Therefore, these data show that decreasing GABA release from a fraction of PV^+ interneurons is sufficient to mediate a large increase in CA3-CA2 excitatory transmission and to allow CA3 input to drive CA2 PN AP firing.

The increase in PSP and PS amplitude observed after CNO application was very similar to what had been reported after induction of DOR-mediated plasticity of inhibitory transmission (Nasrallah et al., 2015). Thus, we wondered whether silencing PV^+ interneurons would prevent the dis-inhibition mediated by DOR agonist application or high-frequency stimulation (HFS) of CA3 input. In control conditions, application of the DOR agonist DPDPE (0.5 μM) or HFS (2 trains of 100 pulses at 100 Hz, 20 s apart) induced a large increase in the amplitude of the PSP from CA3 (Figures 1E and 1F; DPDPE, 221.8% ± 41.9% of baseline, p = 0.026, n = 8; HFS, 230.6% ± 23.2% of baseline, p = 0.0026, n = 6). This increase in CA3 transmission was shown

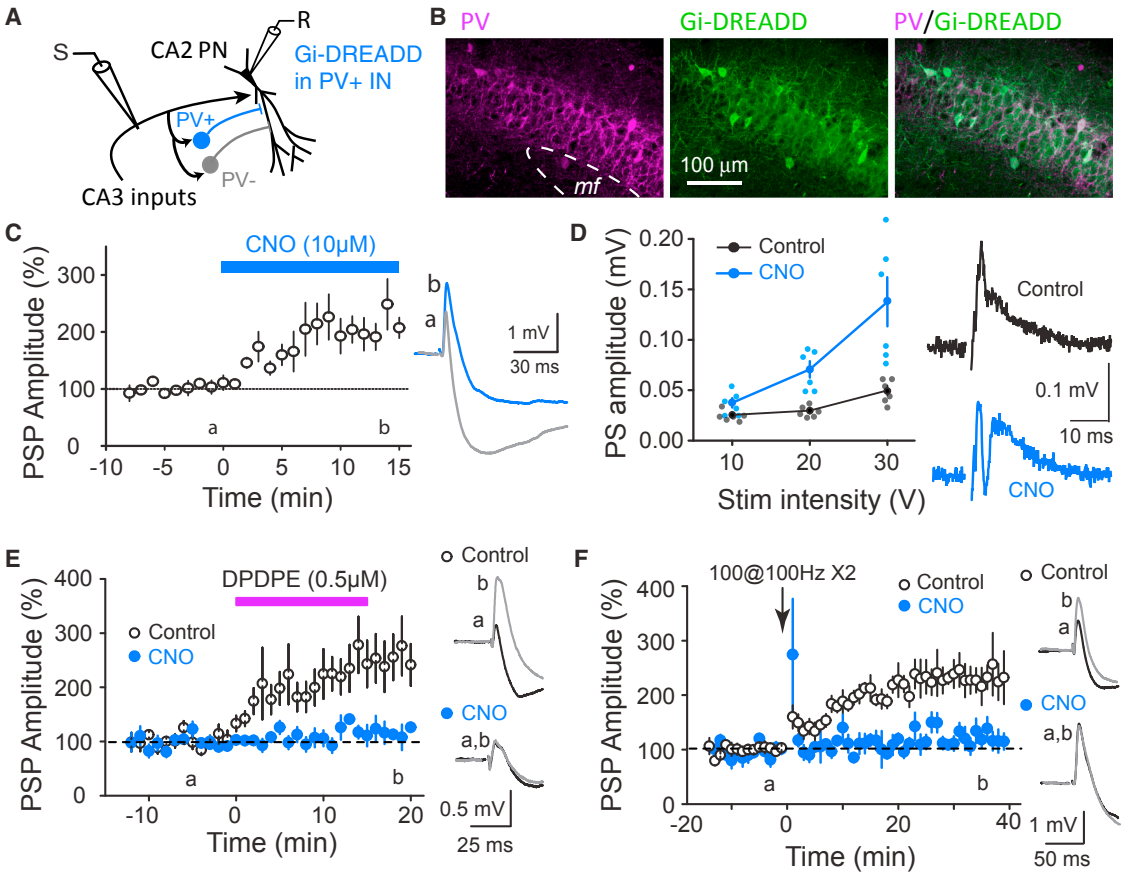

Figure 1. PV$^+$ Interneurons in CA2 Control the Recruitment of CA2 by CA3 and Mediate the DOR-Dependent Dis-inhibitory Increase in CA3 Transmission

(A) Cartoon illustrating the recording conditions. An AAV vector allowing the cre-dependant expression of inhibitory Gi-DREADD was injected into the hippocampus of Pvalb-cre mice. Excitatory transmission from CA3 inputs was monitored in CA2 PNs before and after application of CNO to reduce inhibitory transmission from PV$^+$ interneurons (blue).

(B) Images of area CA2 in a hippocampal slice (mf, mossy fibers) stained for PV (magenta) and for Gi-DREADD (green) showing that most PV$^+$ cells also express Gi-DREADD.

(C) Time course of the normalized amplitude of the depolarizing component of the postsynaptic potential (PSP) recorded in CA2 PNs in response to CA3 input stimulation. Silencing PV$^+$ interneurons with CNO (10 µM) resulted in a large increase in PSP amplitude ($p = 0.003$, $n = 9$). Averaged sample traces corresponding to the time points before (a, gray trace) and after (b, blue trace) CNO application are shown on the right.

(D) Summary graph of the individual experiments and averaged population spike (PS) amplitude as a function of stimulation intensity before (black circles) and after (blue circles) CNO (10 µM) application. Note that silencing PV$^+$ interneurons revealed the emergence of a PS at 20- and 30-V stimulation, as evidenced by the downward deflection on the sample traces in CNO (blue trace).

(E) Time course of the normalized PSP amplitude recorded in CA2 PNs in response to CA3 input stimulation during application of the DOR agonist DPDPE (0.5 µM). In control slices, DPDPE induced a large increase in PSP amplitude (white circles, $p = 0.026$, $n = 8$) but had no effect after silencing PV$^+$ interneurons with CNO (blue circles, $p = 0.21$, $n = 5$). Averaged sample traces corresponding to the time points before (a, black traces) and after (b, gray traces) DPDPE application are shown on the right.

(F) Time course of the normalized PSP amplitude recorded in CA2 PNs in response to high-frequency stimulation of CA3 input. HFS resulted in a large increase in PSP amplitude (white circles, $p = 0.0026$, $n = 6$) in control slices but not in slices with PV$^+$ interneurons silenced by CNO (blue circles, $p = 0.17$, $n = 5$). Averaged sample traces corresponding to the time points before (a, black traces) and after (b, gray traces) HFS are shown on the right. Error bars show SEM.

to be entirely mediated by inhibitory plasticity via a dis-inhibitory mechanism (Nasrallah et al., 2015). When synaptic transmission from PV$^+$ interneurons was reduced by CNO application, the same manipulations had no significant effect on CA3-CA2 transmission (Figures 1E and 1F; DPDPE, 116.3% ± 10.9% of baseline, $p = 0.21$, $n = 5$; HFS, 120.5% ± 12.5% of baseline, $p = 0.17$, $n = 5$). Thus, these data show that PV$^+$ interneurons entirely mediate the DOR-dependent dis-inhibitory increase in CA3 excitatory drive because the increase in PSP resulting from silencing PV$^+$ interneuron transmission fully occluded further effects by HFS or DOR agonist.

Local Plasticity in Area CA2 Controls Information Transfer between CA3 and CA1

We have evidence that inhibitory plasticity of PV$^+$ INs in area CA2 increases excitatory post-synaptic potentials (EPSPs) from CA3

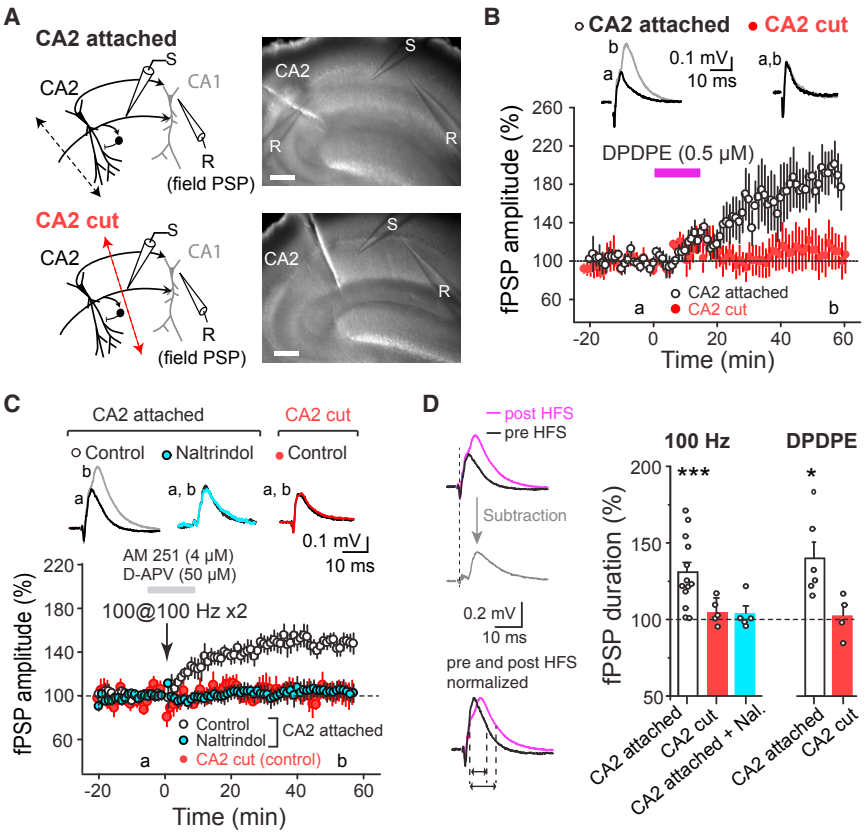

Figure 2. DOR-Mediated Plasticity in Area CA2 Increases Excitatory Drive between CA3 and CA1

(A) Cartoon of the recording conditions and images of acute hippocampal slices that had been cut either between CA3 and CA2 to keep CA2 attached to CA1 (top) or between CA1 and CA2 (bottom). A stimulating electrode (S) was placed in the *stratum radiatum* of CA1 and a recording electrode (R) was placed in the pyramidal layer of CA1. Scale bar, 0.5 mm.

(B) Time course of amplitude of the extracellular field post-synaptic potential (fPSP) during application of the DOR agonist DPDPE. DPDPE (0.5 μM) induced a large increase in fPSP amplitude in slices with CA2 attached to CA1 (white circles, $p = 0.0051$, $n = 7$) but not when CA2 was disconnected from CA1 (red circles, $p = 0.735$, $n = 5$). Averaged sample traces corresponding to the time points before (a) and after (b) DPDPE are shown on top.

(C) Time course of the amplitude of the fPSP in response to HFS of CA3 inputs. HFS led to an increase in fPSP amplitude when CA2 was attached to CA1 in control condition (white circles, $p = 0.000007$, $n = 13$) but not in the presence of the DOR antagonist naltrindole (blue circles, $p = 0.6277$, $n = 5$) or when CA2 was cut from CA1 (red circles, $p = 0.382$, $n = 5$). D-APV (50 μM) was applied 5 min before HFS to prevent NMDA-dependent plasticity at the CA3-CA1 synapses. AM251 (4 μM) was also applied to prevent endocannabinoid-mediated plasticity at inhibitory synapses in CA1. Averaged sample traces corresponding to the time points before (a) and after (b) HFS are shown on top.

(D) Left: sample traces of fPSP recorded before and after HFS. The subtracted trace shows that the component of the fPSP added after HFS is delayed compared with the direct CA3-CA1 fPSP. Right: summary graph of the change in fPSP duration (measured at half amplitude and after normalization, as shown on the bottom traces on the left) in the different experimental conditions. Both HFS and DPDPE induced a significant increase in fPSP duration in control conditions ($p = 0.00043$ and $p = 0.012$, respectively) but not when CA2 was cut or in presence of the DOR antagonist naltrindole (Nal). Error bars show SEM.

and the probability of CA2 firing APs with CA3 stimulation. Because CA3 PNs project to both areas CA2 and CA1, we wondered how the recruitment of CA2 PNs by CA3 affects area CA1. To address that question, we performed extracellular recordings in CA1 *stratum pyramidale* (SP) in hippocampal slices with an incision made either between areas CA2 and CA1 or between areas CA3 and CA2 (Figure 2A). We then evoked iLTD in CA2 by bath application of the DOR agonist DPDPE or by HFS to CA3 inputs. In slices with an incision between CA3 and CA2 (CA2 attached), we found that application of the DOR agonist DPDPE induced a lasting increase in the field post-synaptic potential (fPSP) amplitude in area CA1 (Figure 2B; 188.4% ± 20.9% of baseline, $p = 0.022$, $n = 7$). In contrast, application of DPDPE in slices with an incision between CA2 and CA1 (CA2 cut) led to an increase in the fPSP amplitude during agonist application. This effect was transient, and the fPSP amplitude returned to its initial level upon washout of DPDPE (Figure 2B; 107.42% ± 16.98% of baseline, $p = 0.69$, $n = 5$; $p = 0.018$ with CA2 attached slice). Our results are consistent with the fact that activation of DOR by DPDPE application evokes a lasting decrease in inhibitory transmission in area CA2 but only a transient decrease in area CA1 (Piskorowski and Chevaleyre, 2013). We think that the immediate increase in fPSP we observe with CA2 left intact is due to the quick, yet transient, effect of DOR activation in area CA1 because this was also observed in slices with a cut between area CA1 and CA2. The slower rise in fPSP amplitude in the CA2-attached condition, we think, is from the delayed onset of DOR-mediated plasticity in area CA2.

We also performed similar experiments using HFS instead of DOR agonist application to evoke iLTD in CA2. Because HFS is also well known to induce a NMDA-dependent long-term potentiation (LTP) at the CA3-CA1 excitatory synapses, we applied the NMDA receptor blocker D-2-amino-5-phosphonovalerate (D-APV; 50 μM) during HFS to prevent synaptic plasticity at CA3-CA1 synapses. In most experiments (8 of 13), we also applied the cannabinoid receptor (CB1) blocker AM251 (4 μM) to prevent plasticity at inhibitory synapses in CA1. No differences were found between experiments performed with or without the CB1 receptor blocker; therefore, these experiments were pooled. As expected, we found that HFS did not induce synaptic plasticity when a cut was made between CA2 and CA1 because the fPSP amplitude did not change (Figure 2C; 105.43% ± 8.12% of baseline, $p = 0.382$, $n = 5$). However, we found that the same HFS induced a long-lasting increase in the fPSP

amplitude in area CA1 when connections from area CA2 were intact (Figure 2C; 152.33% ± 6.90% of baseline, p = 0.0018, n = 13, p = 0.0013 with CA2 cut slices). Therefore, this experiment strongly suggests that the increase in CA3-CA1 transmission after HFS results from the recruitment of CA2 PNs after iLTD induction. To confirm the involvement of DOR-mediated iLTD in this process, we performed the same experiment in slices with area CA2 attached to area CA1 (i.e., with a cut between CA3 and CA2) and in the presence of the DOR-selective antagonist naltrindole (0.1 μM). We found that the change in the fPSP amplitude in CA1 was completely abolished in the presence of naltrindole (Figure 2C; 103.04% ± 5.81% of baseline, p = 0.6277, n = 5; p = 0.00073 compared with control). We concluded that the increase in the Schaffer collateral (SC) synaptic drive onto CA1 PNs likely results from the recruitment of CA2 PNs after iLTD induction.

If this interpretation is correct, the excitatory drive coming from CA2 should arrive with a delay compared with the direct CA3-CA1 excitatory transmission. Indeed, when we subtracted the initial fPSP from the fPSP recorded after DPDPE application or HFS, we observed the emergence of a delayed synaptic response (Figure 2D). This delayed response was quantified by an increase in the fPSP duration (measured at half amplitude) after normalizing the fPSP amplitude to the initial response. A significant increase in fPSP duration was observed when CA2 was attached to CA1 after both HFS and DPDPE application (Figure 2D; HFS, from 7.0 ± 0.4 to 9.2 ± 0.7 ms; 130.8% ± 6.4%, n = 13, p = 0.00043; DPDPE, from 5.6 ± 0.6 to 7.8 ± 0.8 ms; 136.5% ± 12.0%, n = 6, p = 0.012). However, these two manipulations did not change the fPSP duration when area CA2 was removed (Figure 2D; HFS, from 6.8 ± 0.2 to 7.2 ± 0.4 ms; 104.3% ± 9.7%, n = 5, p = 0.21; DPDPE, from 6.0 ± 1.0 to 5.9 ± 1.3 ms; 100.7% ± 6.6%, n = 4, p = 0.68). Consistently, HFS resulted in no change in fPSP duration in the presence of the DOR-antagonist naltrindole when area CA2 was attached to CA1 (Figure 2D; from 7.8 ± 0.7 to 8.0 ± 0.5 ms; 104.2% ± 4.6%, n = 5, p = 0.81).

These data indicate that the recruitment of CA2 PNs by CA3 inputs after iLTD results in a significant increase in the excitatory drive between CA3 and CA1. To directly confirm that result in intact slices, we used chemogenetics in combination with the cacng5-cre transgenic mouse line to specifically disrupt CA2 PN transmission. This mouse line has been shown to allow highly specific expression of cre-recombinase-dependent constructs in CA2 PNs after hippocampal viral injection (Boehringer et al., 2017). Virally delivered, cre-driven vector expression is limited to CA2 PNs, as evidenced by the co-localization with the CA2 PN marker PCP4 and exclusion from cells positive for the interneuron marker GAD65/67 (Figure S2). After double-floxed inverse open reading frame (DiO).Gi-DREADD viral injection, we found that DREADD expression was highly specific of CA2 PNs (Figure 3A). We performed whole-cell current-clamp recordings of CA1 PNs and stimulated CA3 SC inputs in the presence of the NMDA receptor blocker D-APV and measured the resulting PSP amplitude. In absence of CNO, HFS induced a significant increase in the PSP amplitude recorded in CA1 PNs in response to SC stimulation (Figure 3B; 134.4% ± 7.4% of baseline, p = 0.0008, n = 12), despite the presence of D-APV to prevent CA3-CA1 plasticity. In contrast, in continuous presence of CNO, and thus reduced CA2 transmission to CA1, HFS did not induce any change in PSP amplitude in CA1 PNs (Figure 3B; 99.1% ± 6.1% of baseline, p = 0.98, n = 6; p = 0.002 with control condition). Therefore, these data further demonstrate that the recruitment of CA2 PNs after local iLTD induction results in an increase in the excitatory drive between CA3 and CA1.

We then explored whether the recruitment of CA2 PNs after local inhibitory plasticity could contribute to AP firing in CA1 PNs with SC stimulation. We used a non-invasive approach by monitoring the amplitude of the PS in the somatic layer of area CA1 before and after application of either HFS or DPDPE (0.5 μM). We performed this measurement in slices with incisions removing either area CA2 or CA3. We found that both HFS and DPDPE application induced a large and long-lasting increase in the CA1 PS amplitude when the recordings were performed in slices with intact area CA2, that is, with a cut separating CA3 (Figures 3C and 3D; HFS, from 192.4 ± 49.8 to 890.5 ± 277.8 μV; 489.6% ± 130.7% of baseline, p = 9.7 10-4, n = 11; DPDPE, from 147.8 ± 17.0 to 735.3 ± 188.3 μV, 516.5% ± 142.7% of baseline, p = 0.03, n = 6). This increase in AP firing did not likely result from a change in CA1 PN intrinsic excitability because no increase in PS amplitude was observed when the incision was between CA2 and CA1 (Figure 3D; HFS, from 248.5 ± 142.9 to 249.1 ± 142.5 μV; 99.6% ± 4.5% of baseline, p = 0.93, n = 5; DPDPE, from 191.7 ± 83.6 to 290.7 ± 110.2 μV; 113.6% ± 7.9% of baseline, p = 0.18, n = 4). Furthermore, we found no significant increase in PS amplitude after HFS in slices with CA2 attached but in the presence of DOR-antagonist naltrindole (Figure 3D; from 285.2 ± 79.1 to 316.6 ± 98.1 μV; 119.4% ± 28.2% of baseline, p = 0.53, n = 5). When using the cacng5-cre mice with Gi-DREADD expression to examine the recruitment of area CA2, we observed no increase in PS amplitude after chemogenetic silencing of CA2 PN transmission with CNO application (Figure 3D; from 139.9 ± 63.0 to 154.5 ± 76.0 μV; 108.5% ± 7.2%, n = 8, p = 0.27).

Because of the increase in CA1 PS after plasticity induction in area CA2, we hypothesized that the recruitment of CA2 PNs by CA3 provides a feed-forward excitatory drive onto CA1 that could influence the temporal fidelity of CA1 AP firing. To test this idea, we performed whole-cell recordings of CA1 PNs and quantified AP firing in response to stimulus trains of CA3 inputs before and after induction of iLTD in CA2. Before iLTD induction with DPDPE, APs were observed in 7 of 14 CA1 PNs during a train at 50 Hz, in 6 of 14 cells with a train of 20 Hz, and in 3 of 14 cells with a train of 10 Hz. After iLTD induction, APs were evoked in most cells at all frequencies: 9 of 14 at 10 Hz, 11 of 14 at 20 Hz, and 12 of 14 at 50 Hz. In AP-firing cells, the probability of firing an AP at each PSP was also significantly increased after inducing iLTD (Figure 3E; at 10 Hz, F = 7.36, p = 0.02; at 20 Hz, F = 12.05, p = 0.005; at 50 Hz, F = 28.01, p = 0.00025). In examining the delay and jitter of the AP before and after iLTD induction, we found that AP delay was significantly reduced (Figure 3F; from 6.77 ± 0.23 ms to 5.43 ± 0.33 ms, n = 8, p = 0.00008) after iLTD induction. Furthermore, the jitter of the AP was also reduced after iLTD induction as measured by the standard deviation of the AP delay (Figure 3F; from 0.77 ± 0.1 to 0.58 ± 0.12, n = 8, p = 0.0066). Altogether, these results

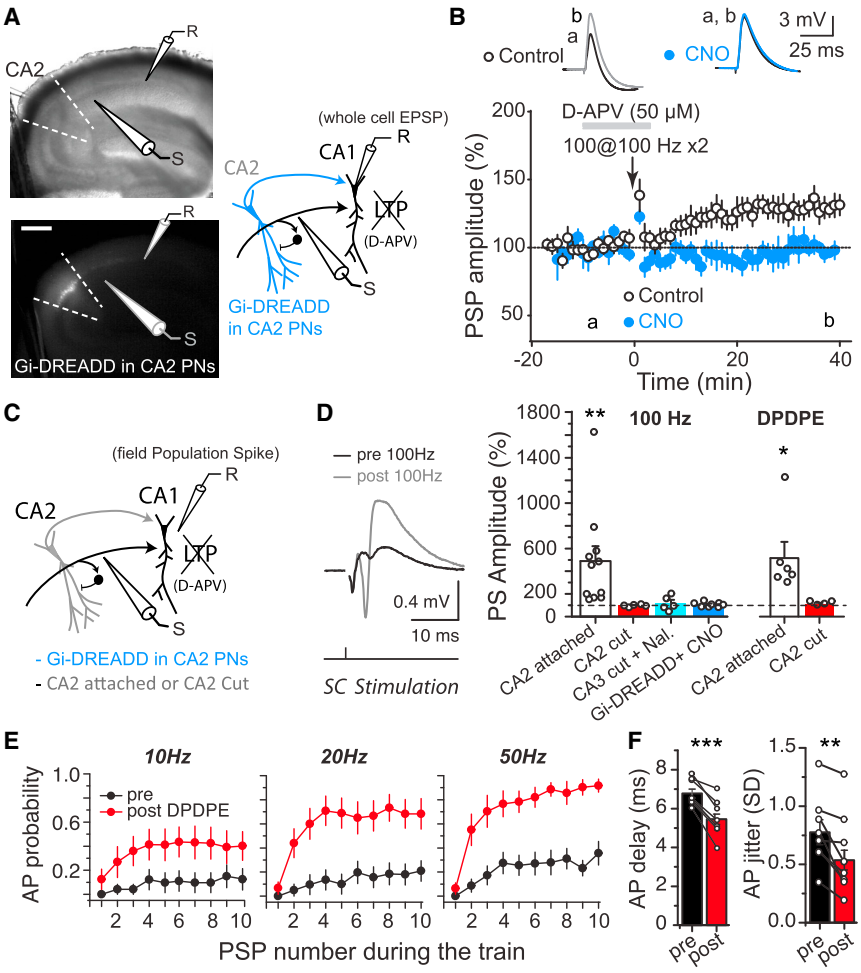

Figure 3. Recruitment of CA2 PNs Mediates the Increase in CA3–CA1 Excitatory Drive and Strongly Increases CA1 Output

(A) Left: recorded hippocampal slice prepared from CACNG5-cre transgenic mouse injected with AAV expressing cre-dependent Gi-DREADD, brightfield image (top) and fluorescence image (bottom) of the same slice showing the expression of inhibitory Gi-DREADD specifically expressed in CA2 PNs. Scale bar, 0.5 mm. Right: cartoon illustrating the recording conditions.

(B) Time course of the normalized amplitude of the PSP in CA1 PNs monitored in whole cells in response to HFS of CA3 inputs. D-APV was applied just before HFS to prevent NMDA-dependent plasticity at CA3-CA1 synapses. In control slices, HFS led to a significant increase in the PSP amplitude (white circles, p = 0.0008, n = 12). This increase resulted from the recruitment of CA2 PNs because it was completely prevented when CA2 PNs were silenced with CNO (blue circles, p = 0.98, n = 6). Averaged sample traces corresponding to the time points before (a, black traces) and after (b, gray control and blue with CNO) HFS are shown above.

(C) Left: cartoon of the stimulating and recording conditions. The population spike was monitored in the pyramidal layer of CA1 in response to CA3 inputs stimulation after HFS or DPDPE application in diverse conditions: area CA2 attached (CA3 cut) in control or in presence of DOR-antagonist naltrindole, area CA2 disconnected from CA1 (CA2 cut) or CA2 PNs expressing Gi-DREADD and silenced with CNO.

(D) Left: sample traces of fPSP recorded in the pyramidal layer in CA1 before and after HFS. Note the large increase in the PS after HFS. Right: summary graph of the change in PS amplitude after HFS or DPDPE application in diverse experimental conditions. An increase in PS is observed in slices where CA2 was attached to CA1 after HFS (p = 0.00097, n = 5) and after DPDPE application (p = 0.03, n = 6), but not when CA2 was cut from CA1 (HFS: p = 0.46, n = 5; DPDPE p = 0.93, n = 4), when DOR receptors were blocked with naltrindole (Nal.; p = 0.53, n = 5) or when CA2 PNs were silenced (p = 0.27, n = 8).

(E) Summary graph of the AP probability measured in CA1 PNs in response to stimulation trains of CA3 inputs at 10, 20, and 50 Hz before (black) and after (red) iLTD induction with DPDPE application.

(F) Summary of the delay and jitter (measured as the standard deviation of the delay) of the AP during the 50 Hz stimulation train before and after iLTD induction. DPDPE application induced a decrease in AP delay (p = 0.00008, n = 8) and a decrease in AP jitter (p = 0.0066, n = 8). Error bars show SEM.

show that a locally constrained and lasting plasticity of inhibitory transmission of PV^+ interneurons allows CA2 PNs to be recruited by CA3 activity, resulting in an enhanced multi-synaptic excitatory drive onto CA1 PNs, which increases the probability and temporal fidelity of CA1 PN AP firing with a shorter delay and reduced jitter.

Feed-forward Inhibition Normalizes the Excitatory Drive from CA2 onto Deep and Superficial CA1 PNs

There is evidence that deep (with soma closer to *stratum oriens*) and superficial (with soma closer to *stratum radiatum*) CA1 PNs are morphologically, physiologically, and functionally distinct (Bannister and Larkman, 1995; Lee et al., 2014; Mizuseki et al., 2011; Soltesz and Losonczy, 2018). Furthermore, it has been shown that deep CA1 PNs receive stronger excitatory drive from CA2 compared with superficial CA1 PNs (Kohara et al., 2014). We postulated that after activity-dependent iLTD and recruitment of CA2 PNs, the increase in PSP in deep CA1 PNs should be greater than it is in superficial CA1 PNs. To address that question, we performed whole-cell current-clamp recordings of deep and superficial CA1 PNs before and after HFS to evoke iLTD in area CA2. The recorded cells were filled with biocytin, and their location as deep or superficial in the pyramidal layer was precisely determined by staining of the filled cell as well as the soma in the pyramidal layer and performing confocal microscopy (Lee et al., 2014). Surprisingly, we found that the increase in PSP amplitude after HFS was not greater in deep (Figure 4A; 129.8% ± 11.8% of baseline, p = 0.04, n = 6) as compared with superficial CA1 PNs (Figure 4A; 135.6% ± 10.0% of baseline, p = 0.015, p = 0.37 with deep CA1 PNs, n = 6). To better assess the synaptic component due to the recruitment of CA2 PNs, we subtracted the PSP before HFS from the PSP monitored after HFS (Figure 4A). We found that the subtracted PSPs had similar amplitude in deep

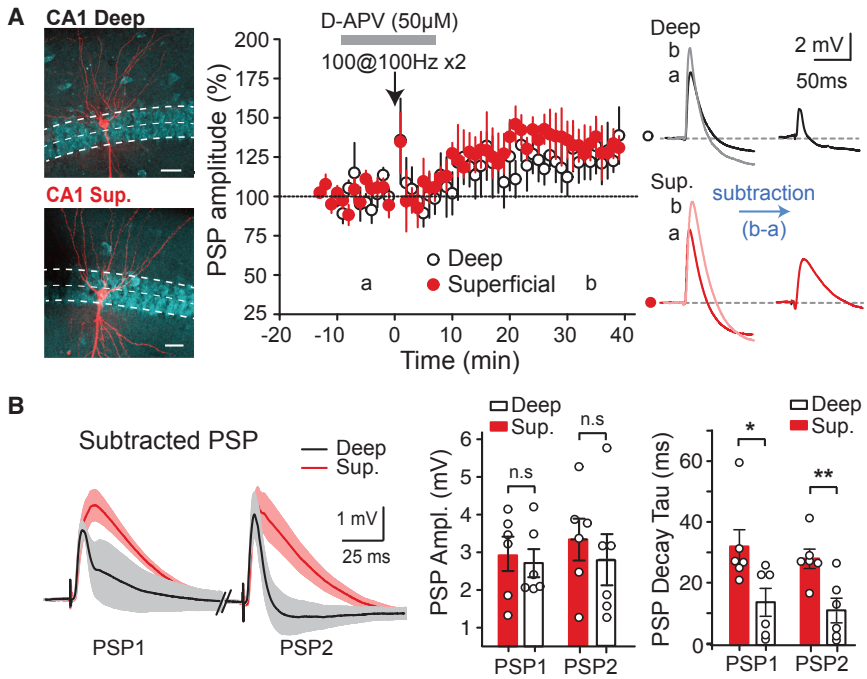

Figure 4. Activity-Dependent Recruitment of CA2 PNs Does Not Provide a Larger Excitatory Drive onto Deep, Compared with Superficial, CA1 PNs

(A) Left: sample images of biocytin-filled CA1 PNs (red) recorded during application of HFS in intact slices. Neuronal cells were stained with Nissl to determine the location of the recorded CA1 PN (above, a deep CA1; below, a superficial CA1 PN). Middle: time course of the PSP amplitude monitored in a whole-cell recording of deep or superficial CA1 PNs. Note that the increase in PSP amplitude is similar in both populations of CA1 neurons. Averaged sample traces corresponding to the time points before (a) and after (b) HFS are shown on the right. The trace before HFS was subtracted from the trace after HFS to isolate the component added by recruitment of CA2 PNs. Scale bar: 30 μm.

(B) Left: averaged PSPs (± SEM) during a paired-pulse stimulation obtained after subtraction, as displayed in (A) for deep and superficial CA1 PNs. Note that, although the amplitudes are similar, the decay of the PSPs decay time courses differ between deep and superficial PNs. Right: summary graph of the averaged values (± SEM) and individual cell values for the PSP amplitude and PSP decay. The amplitudes were not different between deep and superficial cells (PSP1, p = 0.68; PSP2, p = 0.55, n = 6), but the decays were faster in deep CA1 PNs (PSP1, p = 0.03; PSP2, p = 0.008, n = 6).

(Figure 4B; PSP1, 2.7 ± 0.4 mV, n = 6; PSP2, 2.8 ± 0.7 mV, n = 6) and superficial (Figure 4B; PSP1, 3.0 ± 0.5 mV, p = 0.68 with deep CA1, n = 6; PSP2, 3.4 ± 0.6 mV, p = 0.55 with deep CA1, n = 6) CA1 PNs. However, the time course of the decay of the subtracted PSP was significantly faster in deep CA1 PNs (Figure 4B; PSP1, τ_{deep} = 13.5 ± 4.6 ms, n = 6; $\tau_{superficial}$ = 31.7 ± 5.7 ms, p = 0.03, n = 6; PSP2, τ_{deep} = 10.8 ± 4.0 ms, n = 6; $\tau_{superficial}$ = 27.8 ± 3.2 ms, p = 0.008, n = 6). Therefore, these data suggest that the PSP from CA2 might be controlled by a larger feed-forward inhibition in deep, as compared with superficial, CA1 PNs.

With optogenetics and whole-cell voltage-clamp recordings, it was shown that the amplitude of the excitatory post-synaptic currents (EPSCs) between CA2 and CA1 was not controlled by feed-forward inhibition (Kohara et al., 2014). To more precisely examine the influence of feed-forward inhibition on excitatory drive at the CA2-CA1 synapse, we chose to perform current-clamp recordings of CA1 PNs. We used the cacng5-cre mouse line to selectively express channelrhodopsin-2 (ChR2) in CA2 PNs and monitored the light-evoked changes in membrane potential in deep and superficial CA1 PNs in control conditions and after blocking inhibitory transmission (Figure 5A). We monitored the amplitude of the depolarizing component of the PSP over a wide range of light-stimulation intensities. We found that in control conditions, the depolarizing component of the PSP was not significantly different between deep and superficial CA1 PNs (Figures 5B and 5D; at 15 mW/mm^2, superficial, 2.49 ± 0.52 mV, n = 8; deep, 4.22 ± 0.95 mV, n = 7; p = 0.093). However, in agreement with our previous results, we found that the decay of the PSP was significantly faster in deep, as compared with superficial, CA1 PNs (Figure 5D; at 15 mW/mm^2, superficial, 19.6 ± 2.6 ms, n = 8; deep, 12.3 ± 1.5 ms, n = 7; p = 0.039). In the presence of $GABA_{A\&B}$ receptor antagonists, the amplitude of PSPs became significantly greater in deep, compared with superficial, CA1 PNs (at 15 mW/mm^2, 8.52 ± 1.9 mV versus 3.36 ± 0.8 mV; p = 0.042). Conversely, blocking $GABA_{A\&B}$ receptors abolished the difference in the decay-time constant of the EPSP between deep and superficial CA1 PNs (Figure 5D; at 15 mW/mm^2, 26.03 ± 3.04 ms versus 24.02 ± 3.8 ms; p = 0.69). To isolate the inhibitory component evoked by stimulation of CA2 PNs onto CA1 PNs, we subtracted the responses before and after application of $GABA_{A\&B}$ receptor antagonists. We found that the isolated IPSP was, on average, four times greater in deep CA1 PNs as compared with superficial CA1 PNs (Figure 5E; deep, 4.8 ± 1.1 mV, n = 7; superficial, 1.0 ± 0.24 mV, n = 8; p = 0.012). Altogether, these data show that CA2 PNs recruit a stronger feed-forward inhibition onto deep, compared with superficial, CA1 PNs. This feed-forward inhibition acts to normalize the amplitude of the PSP from CA2 onto deep and superficial CA1 PNs.

It is unclear why the isolated excitatory drive from CA2 is stronger onto deep CA1 compared with superficial CA1 PNs. In contrast to the monosynaptic contact between CA3 and CA1 PNs, it has been shown that a single CA2 PN can make several synapses on a single CA1 PN (Chevaleyre and Siegelbaum, 2010). Therefore, one possible explanation could be that deep CA1 PNs receive more synapses than superficial CA1 PNs. CA2 PNs mainly send their projections in *stratum oriens* of CA1 (see Figure 5B). Thus, we reconstructed deep and superficial CA1 PNs and quantified the morphology of the basal dendrites.

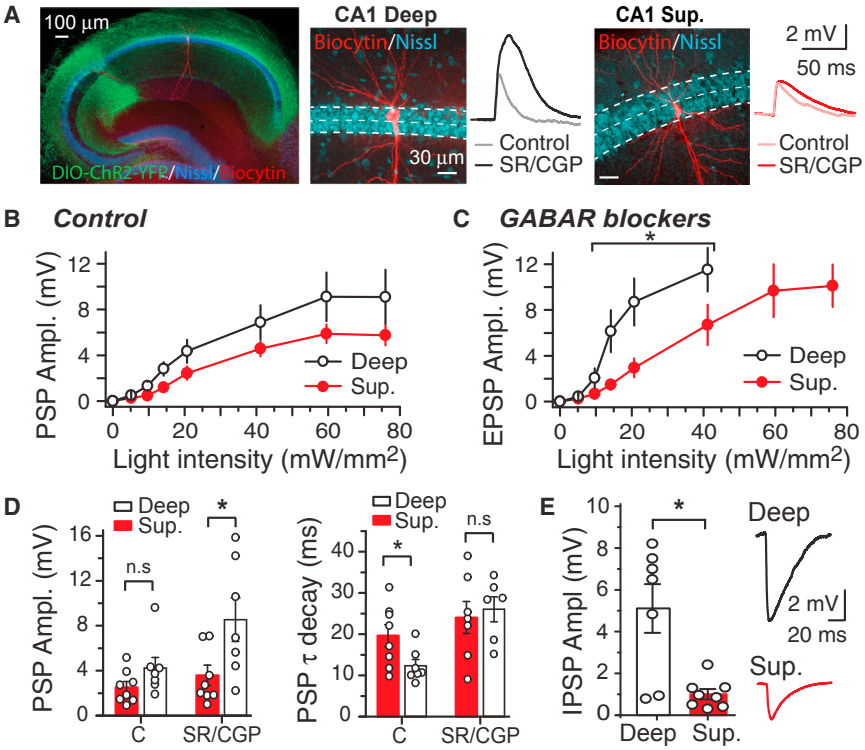

Figure 5. Recruitment of Feed-Forward Inhibition Normalizes the Excitatory Drive from CA2 onto Deep and Superficial CA1 PNs

(A) Image of a hippocampal slice from the CACNG5-cre mouse line injected with AAV expressing cre-dependent channelrhodopsin (ChR2). The expression of ChR2 (green) was restricted to CA2 PN membrane, visible in soma and dendrites in area CA2 and CA2 axons in areas CA3 and CA1. Recorded CA1 PNs were filled with biocytin (red) and subsequently stained. All neuronal soma were stained with Nissl (blue). Sample images of a deep and a superficial CA1 PN and their respective responses to light stimulation of CA2 PNs before and after blocking inhibitory transmission with the $GABA_{A\&B}$ blockers SR95531(1 μM) and CGP 5584A (2 μM) (SR/CGP). (B and C) Summary graphs of the amplitude of the PSP evoked by different intensities of light in deep and superficial CA1 PNs before (B) or after blocking inhibitory transmission with $GABA_{A\&B}$ blockers (C). PSP amplitudes are not different in the control conditions ($p = 0.093$) but are significantly different after blocking GABA transmission ($p = 0.042$).

(D) Summary graph and individual cell values for the PSP amplitude and decay time constant obtained with a stimulation of 21 mW/mm^2. In control conditions (C), the PSP amplitudes were not different between deep and superficial CA1 PNs ($p = 0.09$, $n = 8$ superficial, $n = 7$ deep), but the decay was faster in deep CA1 PNs ($p = 0.036$). After blocking inhibition with SR95531 (1 μM) and CGP 5584A (2 μM) (SR/CGP), the PSP amplitude became larger in deep, compared with superficial, CA1 PNs ($p = 0.042$), and the decay became similar in deep and superficial CA1 PNs ($p = 0.16$).

(E) Summary graph and individual cell values of the inhibitory component evoked by CA2 PN stimulation obtained by subtracting the traces in control conditions (C) from the traces recorded in GABA receptor blockers (SR/CGP). The amplitude of the IPSP was significantly larger in deep CA1 PNs ($p = 0.012$). Averaged sample traces of the IPSP in deep and superficial cells are shown on the right. Error bars show SEM.

We found a significant correlation between the location of the CA1 PN along the radial axis of the somatic layer and the number of basal dendritic branches. Specifically, although the number of primary basal dendrites was similar between deep and superficial CA1 PNs, we found that cells located closer to *stratum oriens* (SO) had more higher-ordered dendrites, nodes, and branch endings as compared with cells located closer to the *stratum radiatum* (SR; Figure S3). The total length of dendrites located in the SO was also significantly greater for deep, compared with superficial, CA1 PNs. Therefore, these data provide a potential explanation for the stronger excitatory drive from CA2 onto deep CA1 PNs.

In addition to deep and superficial CA1 PNs, we also recorded large neurons with soma in SR (Figure 6A). These neurons, called radiatum giant cells (RGCs), have previously been described as being excitatory (Gulyás et al., 1998) and are known to differ from CA1 PNs by their inversed expression gradient of hyperpolarized-activated cation channel, HCN (Bullis et al., 2007). Furthermore, RGCs have been found to have an increased contribution of NMDA in the EPSP evoked by SR stimulation as compared with EPSPs in CA1 PNs (Kirson and Yaari, 2000). After reconstruction of these cells, we observed a cellular morphology very consistent with what has previously been described for these neurons (Figure 6B), displaying two thick apical dendrites and having a soma with an inverted, triangular shape. Furthermore, consistent with what has been described, the basic intrinsic electrophysiological properties during depolarizing or hyperpolarizing pulses were similar to that of CA1 PNs (Figure 6C). Surprisingly, we found that light stimulation of CA2 PN axonal fibers resulted in large PSPs that were significantly larger than the PSPs of superficial CA1 PNs (at 41 mW/mm^2, 7.7 ± 1.3 mV for RGC; and 4.6 ± 0.67 mV for superficial CA1 PNs; $p = 0.043$) but similar in magnitude to those of deep CA1 PNs (at 41 mW/mm^2, 6.9 ± 1.5 mV; $p = 0.70$). After blocking inhibitory transmission by applying $GABA_{A\&B}$ receptor blockers, the PSP amplitude of RGCs was significantly increased (at 41 mW/mm^2, from 7.7 ± 1.3 to 12.41 ± 2.07, $p = 0.045$, $n = 6$) and stimulation with light intensities greater than 20 or 40 mW/mm^2 often led to AP firing (Figure 6D). These data provide evidence that CA1 RGCs are strongly connected both directly by CA2 PN axons and indirectly by feed-forward inhibition from CA2 PNs.

PV^+ Interneurons Control CA2 Input onto Deep and SR CA1 PNs

Deep CA1 PNs have been shown to receive more inhibitory transmission from PV^+ basket cells compared with superficial CA1 PNs (Lee et al., 2014). It is unknown whether intra-hippocampal projections from CA2 PNs recruit PV^+ basket cells in area CA1. To answer that question, we took advantage of the finding that

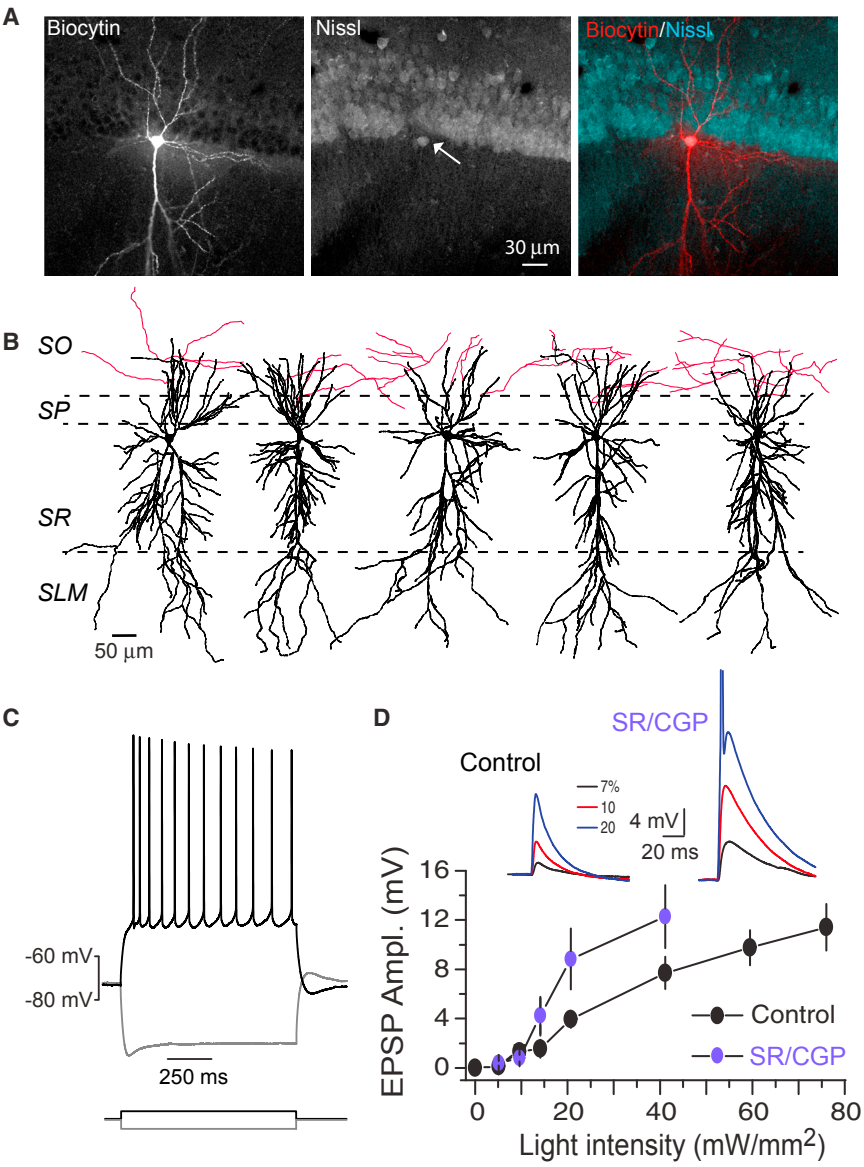

Figure 6. CA2 PNs Provide a Strong Connection onto CA1 RGCs

(A) Image of a recorded neuron filled with biocytin (left), Nissl staining of all neuronal soma (middle), and an overlay (right) showing the location of the soma just below the cell body layer in *stratum radiatum*.

(B) Reconstruction of recorded radiatum giant cells (RGCs; dendrites are in black; axons are in red). Note the presence of two apical dendrites emerging from the soma or one apical dendrite branching into two thick dendrites close to the soma.

(C) Voltage responses elicited by hyperpolarizing and depolarizing current injections (shown below) illustrating that RGCs have a firing pattern similar to CA1 PNs.

(D) Summary graph of the amplitude of the PSP recorded in RGCs evoked by different light intensities in a CACNG5-cre mouse line expressing ChR2 in control conditions (black circles) and after blockade of inhibitory transmission with SR95531 (1 μM) and CGP 5584A (2 μM) (SR/CGP); purple circles). In the presence of GABA receptor blockers, PSP amplitude could not be quantified above 40 mW/mm^2 because of the occurrence of action potential firing. Averaged sample traces at three light intensities are shown above. Error bars show SEM.

synaptic transmission from PV$^+$ interneurons was nearly entirely lost after activation of mu opioid receptors (MORs) (Glickfeld et al., 2008). We selectively expressed ChR2 in CA2 PNs and monitored the PSP amplitude in all three classes of CA1 PNs before and after applying the MOR agonist DAMGO (1 μM). We found that the DAMGO application induced a large and significant increase in PSP amplitude in deep (at 15 mW/mm^2, 94.6% ± 36.2%, p = 0.047) and in RGCs (87.7% ± 14.6%, p = 0.0035), but not in superficial CA1 PNs (27.4% ± 18.3%; p = 0.2; Figure 7A). Similarly, the PSP decay became much slower after DAMGO application in deep (87.4% ± 8.3%; p = 0.00045) and RGCs (62.2% ± 16.2%; p = 0.018), but not in superficial CA1 PNs (3.3% ± 7.2%; p = 0.67; Figure 7A). Subsequent blockade of all inhibitory transmission with SR/CGP had no significant additional effect on PSP amplitude (deep, 104.2% ± 38.8%, p = 0.067 with DAMGO; superficial, 18.1% ± 8.4%, p = 0.49 with DAMGO; RGC, 120.5% ± 96.3%, p = 0.47 with DAMGO). Application of GABA$_{A\&B}$ receptor blockers also had no additional effect on EPSP decay in deep and superficial CA1 PNs (deep, 128.8% ± 33.4%, p = 0.18 with DAMGO; superficial, 10.1% ± 13.7%, p = 0.60 with DAMGO) and induced a small, but significant, increase in RGCs (155.9% ± 32.6%, p = 0.045 with DAMGO). These data show that most of the control of the EPSP by feed-forward inhibition between CA2 and both deep CA1 PNs and RGCs is mediated by PV$^+$ interneurons.

Finally, because we observed an increase in the PS in CA1 after recruitment of CA2 by CA3 inputs, we next wondered which subset of CA1 PNs was able to fire APs upon CA2 stimulation and whether feed-forward inhibition from PV$^+$ interneurons was effective at controlling AP firing. In control conditions, stimulation of CA2 inputs could evoke APs in some deep PNs and RGCs (deep, 2 of 5; RGCs, 1 of 5) but never in superficial CA1 PNs (0 of 7). After blocking transmission from PV$^+$ interneurons with DAMGO, light activation of CA2 PN axons was able to evoke AP firing in most deep CA1 PNs and RGCs (deep, 3 of 5; RGCs, 3 of 5), but not in superficial CA1 PNs (0 of 7). Blocking all inhibition further increased the proportion of deep CA1 PN- and RGC-firing APs (deep, 4 of 5; RGCs, 4 of 5) and revealed AP firing in some superficial CA1 PNs (2 of 7). The average number of APs was significantly increased after blocking inhibitory transmission compared with control conditions in deep

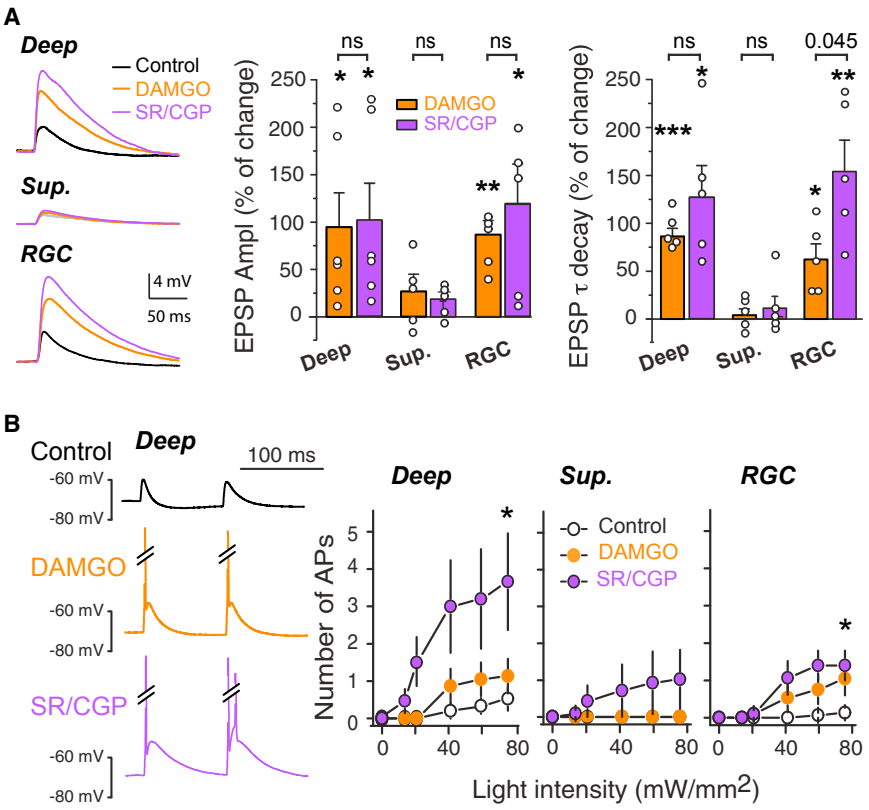

Figure 7. PV⁺ Interneuron-Mediated Feed-Forward Inhibition from CA2 PNs Tightly Controls EPSP and Action Potential Firing in Deep PNs and RGCs

(A) Summary graph for the quantification of the change in amplitude and decay of the PSP evoked by 15 mW/mm^2 light stimulation of CA2 PNs and recorded in deep, superficial, and RGC CA1 PNs after application of the Mu opioid receptor agonist DAMGO (orange) and application of the $GABA_{A\&B}$ receptor blockers SR95531 (1 μM) and CGP 5584A (2 μM) (SR/CGP) (purple). Averaged sample traces are shown on the left. Application of DAMGO (1 μM) induced a significant increase in PSP amplitude and decay in deep ($p = 0.047$ and $p = 0.00045$, respectively) and RGC CA1 PNs (amplitude: $p = 0.0035$; decay: $p = 0.018$) but not in superficial CA1 PNs. Subsequent application of $GABA_{A\&B}$ receptor blockers slightly but non-significantly increased the PSP amplitude and decay in deep PNs and significantly increased EPSP decay in RGCs ($p = 0.045$).

(B) Left: example traces of synaptic response to a paired stimulation of CA2 axons with light in a deep CA1 PN. In control conditions, no APs were evoked by the stimulation. Application of DAMGO resulted in AP firing, and more APs are observed after complete block of inhibitory transmission by SR/CGP. Right: summary graph of the number of APs evoked in deep, superficial, and SR CA1 PNs in control conditions and after application of DAMGO and SR/CGP. DAMGO induced a non-significant increase in the number of action potentials in deep CA1 PNs and RGCs. Subsequent application of $GABA_{A\&B}$ receptor blockers further increased the AP number in deep ($p = 0.045$ with control) and RGC PNs ($p = 0.012$ with control). Error bars show SEM.

PNs (Figure 7B; at 76 mW/mm^2, from 0.46 ± 0.28 to 3.66 ± 1.29, $p = 0.045$, $n = 5$) and in RGCs (at 76 mW/mm^2, from 0.13 ± 0.13 to 1.4 ± 0.4, $p = 0.012$, $n = 5$) but not in superficial CA1 PNs (at 76 mW/mm^2, from 0 to 1.02 ± 0.8, $p = 0.37$ $n = 7$). The fact that a few superficial cells (2 of 7) fired AP after blockade of inhibitory transmission, despite the lack of effect of GABAR blockers on EPSP amplitude (Figure 7A), can be explained by the different stimulation intensities used in these experiments. We used a small-intensity stimulation (15 mW/mm^2) to monitor the change in EPSP amplitude and decay because greater stimulations led to AP firing in most deep cells, thus precluding an accurate measure of the EPSP. At greater stimulation intensities (>20 mW/mm^2), GABA blockers led to a small, but non-significant, increase in PSP amplitude (see Figures 5B and 5C) and revealed AP firing in a small fraction of superficial cells. Altogether, these data reveal that CA2 PN inputs are sufficient to evoke APs onto deep and CA1 PNs and RGCs, and that drive is strongly controlled by feed-forward inhibitory transmission (see model in Figure S4).

DISCUSSION

In this study, we identified a synaptic target of CA2 PNs in the hippocampus and revealed how large feed-forward inhibition controls both the recruitment of CA2 PNs and the excitatory drive between CA2 and CA1. First, we found that PV⁺ interneurons strongly contribute to the inhibitory control of CA2 PNs and entirely underlie the DOR-dependent dis-inhibition of CA2 PNs. Second, we found that local inhibitory plasticity in area CA2 allows the recruitment of CA2 PNs by CA3 input and increases the excitatory drive between CA3 and CA1. Third, we found that feed-forward inhibition normalizes the excitatory drive from CA2 onto deep and superficial CA1 PNs. Fourth, we show that PV⁺ interneurons largely contribute to the feed-forward inhibition from CA2 to CA1. Finally, we reveal that RGCs located in area CA1 SR are strongly connected directly by CA2 PNs and indirectly by CA2-mediated feed-forward inhibition.

Role of PV⁺ Interneurons in Controlling Recruitment of CA2 PNs by CA3 Inputs

In contrast to excitatory inputs from CA3, inhibitory transmission in area CA2 is plastic and displays an LTD mediated by DOR activation. We have shown that this plasticity mediates a dis-inhibitory increase in CA3 transmission and allows CA3 inputs to recruit CA2 PNs (Nasrallah et al., 2015). PV⁺ interneurons have recently been shown to mediate an input-timing-dependent plasticity evoked by pairing cortical and CA3 input stimulations (Leroy et al., 2017). It was unclear, however, whether the same interneuron population was involved in the dis-inhibitory increase in CA2 output mediated only by CA3 activity. Using chemogenetics, we showed that silencing PV⁺ interneuron

transmission was sufficient to increase the amplitude of the PSP from CA3 and permit CA2 PNs to fire APs. Silencing inhibitory transmission from PV^+ interneurons completely occluded any subsequent increase in CA3 excitatory drive by HFS or pharmacological DOR activation. Therefore, our data demonstrate that PV^+ interneurons mediate all the dis-inhibitory increase in CA3-CA2 transmission and reveal that PV^+ interneurons have a critical role in controlling recruitment of CA2 PNs and information transfer within the hippocampus.

Given the role of CA2 PNs in social memory formation (Hitti and Siegelbaum, 2014), this finding has pathological relevance. PV^+ interneuron density has been found to be decreased in the hippocampus uniquely in area CA2 in post-mortem studies of schizophrenic patients (Knable et al., 2004) and in a mouse model of the 22q11.2 deletion syndrome (Piskorowski et al., 2016). Consistently, a decrease in DOR-mediated iLTD was observed in mice with the 22q11.2 deletion, along with decreased AP firing of CA2 PNs after iLTD induction (Piskorowski et al., 2016). Therefore, our results highlight a critical role of PV^+ interneurons in area CA2 and reveal how a decreased PV^+ interneuron density in that area might explain the deficit observed during neuropsychiatric diseases with impaired social cognition.

Recruitment of CA2 PNs Increases the Excitatory Drive between CA3 and CA1

To examine the extent to which the recruitment of CA2 PNs by CA3 after iLTD of PV^+ interneuron transmission alters the drive onto CA1, we disrupted the transmission from CA2 by two different methods. We made very small incisions in hippocampal slices to physically separate the input from CA2 PNs in the slice or left area CA2 intact. We also used a CA2-specific transgenic line, cacng5-cre, and performed targeted viral injections to express silencing Gi-DREADD in CA2 PNs. Our data show that induction of DOR-mediated iLTD in area CA2 contributes to the excitatory drive between CA3 and CA1. Indeed, after iLTD induction in area CA2, the trisynaptic pathway that normally bypasses CA2 because of large feed-forward inhibition can recruit CA2 PNs. This added an additional di-synaptic connection between CA3 and CA1 (i.e., CA3-CA2-CA1) and resulted in an increase in the excitatory drive of SC stimulation onto CA1 PNs. Even when the LTP between SC and CA1 PNs is blocked, HFS of SC or pharmacological manipulations that reduce inhibitory transmission in CA2 increased EPSP amplitude in CA1 PNs. The emergence of a delayed di-synaptic component was clearly visible on the PSP recorded extracellularly in the somatic layer of CA1.

This finding has an important implication: when synaptic transmission and plasticity at CA3-CA1 synapses is studied in intact slices, one has to be careful that any manipulation that affects EPSPs in CA1 is not an indirect consequence of the recruitment of CA2 PNs. For instance, it was shown that blockade of inhibitory transmission reveals a delayed response in CA1 PNs, an effect that was interpreted as being mediated by recurrent connections between CA1 PNs (Crépel et al., 1997). Although we do not challenge that interpretation, our results also provide another mechanism by which blocking inhibitory transmission could reveal a delayed EPSP in CA1 PNs from CA3 stimulation. Similarly, a delayed response was also observed in CA1 PNs after blocking adenosine receptors with the A1 receptor blocker cyclopentyltheophylline (CPT) (Klishin et al., 1995). Interestingly, the concentration of CPT used in this study (100 nM) was shown later on to have no effect on CA3-CA1 transmission but to trigger a large increase in CA3-CA2 EPSPs (Simons et al., 2011). Although a cut was made in the slice to prevent activation of CA3, it is possible that if CA2 were left intact, part of the effect observed might have been mediated by the recruitment of CA2 PNs.

Feed-forward Inhibition Normalizes Excitatory Drive from CA2 onto Deep and Superficial CA1 PNs

With optogenetic activation of CA2 PNs, it has been shown that light-evoked excitatory currents recorded in CA1 PNs were stronger in deep, than in superficial, CA1 PNs (Kohara et al., 2014). Furthermore, larger EPSCs onto deep CA1 PNs have also been reported with extracellular activation of CA2 PNs (Valero et al., 2015). Consistent with our results, this study also reported larger feed-forward inhibitory currents onto deep CA1 PNs. Neither of the two previous works examined the effect of CA2-driven feed-forward inhibition on the excitatory potentials of CA1 PNs. Here, we made the unexpected finding that when CA1 PNs were not voltage-clamped, the amplitude of EPSPs from CA2 PNs was not significantly larger in deep, as compared with superficial, cells. However, the decay time course was significantly faster in deep CA1 PNs, revealing that feed-forward inhibition is acting to control EPSP shape and amplitude only in deep CA1 PNs. Indeed, blocking inhibitory transmission slowed the decay of EPSPs in deep CA1 PNs and increased their amplitude, but it did not affect EPSPs in superficial CA1 PNs. We postulate that this difference in EPSC amplitude between deep and superficial cells is potentially a consequence of the increased dendritic length and number of branches in deep cells as compared with superficial PNs. As previously reported in mice (Lee et al., 2014), we observed an increased dendritic length in SO in deep CA1 PNs. Furthermore, in agreement with what has been described in rats (Bannister and Larkman, 1995), we also observed that deep CA1 PNs have more dendritic branches than superficial CA1 PNs.

The fact that a previous study did not observed any effect of inhibition on CA2-CA1 excitatory transmission likely results from the recording method (Kohara et al., 2014). Indeed, the CA2-CA1 transmission was monitored in voltage-clamp at −70 mV. This recording configuration will greatly minimize any contribution of inhibitory transmission. With a more physiological recording configuration, we show that CA2-CA1 transmission is strongly controlled by feed-forward inhibition in deep, but not in superficial, CA1 PNs. This inhibition acts to normalize the excitatory drive onto deep and superficial CA1 PNs.

We postulate that this feed-forward inhibition recruited by CA2 inputs may have a role in the microcircuit that controls the participation of different populations of CA1 PNs during hippocampal function. Differences in activity have been reported in deep and superficial CA1 PNs during theta and gamma oscillations *in vivo* (Mizuseki et al., 2011; Senior et al., 2008). It has been shown that during sharp-wave ripple (SWR) events,

deep CA1 PNs have hyperpolarized membrane potentials, whereas superficial PNs are depolarized, and the participation of CA1 PNs in SWR activity *in vivo* correlates with somatic location (Valero et al., 2015). Further, a fraction of SWRs have been shown to originate from oscillatory activity in area CA2 (Oliva et al., 2016). In that study, the authors propose that interneurons in area CA1 are activated by CA2 inputs during the SWR event. Our data support that hypothesis and demonstrate directly that CA2 PNs engage feed-forward inhibition in area CA1, particularly onto deep CA1 PNs. Which population of interneurons is responsible and the contribution to the overall circuit remain open questions.

CA2 PNs Strongly Connect RGCs in Area CA1

Our results reveal a post-synaptic target of CA2 PNs within the hippocampus. We found that CA2 PNs strongly connect to large neurons in area CA1 SR. Although little is known about these cells, they were originally characterized and named radiatum giant cells (RGCs) by Gulyás et al. (1998). Their dendritic branching is similar to CA1 PNs but with some characteristic differences, often having two large, apical dendrites or one apical dendrite that bifurcates close to the soma, and these apical dendrites form a large dendritic tuft in *stratum lacunosum-moleculare* (SLM) (Gulyás et al., 1998). Like classical CA1 PNs, their excitatory inputs display a NMDA-dependent LTP in response to a pairing protocol. However, they differ from classical CA1 PNs by a large contribution of NMDA receptors to synaptic responses evoked by stimulation in SR (Kirson and Yaari, 2000). They also express a reversed gradient in HCN channels compared with other CA1 PNs (Bullis et al., 2007). Although electrical stimulation in SR has been shown to evoke EPSPs in RGCs, that kind of stimulation cannot discriminate between CA3 and CA2 inputs. Using specific optogenetic stimulation of CA2 PNs, we show here that CA1 RGCs are strongly connected by CA2 PNs. The physiological relevance of the strong connection between CA2 and CA1 RGCs is currently unknown. Interestingly, RGCs in the ventral hippocampus have been shown to project directly to the olfactory bulb (Gulyás et al., 1998; van Groen and Wyss, 1990). Silencing transmission from CA2 PNs resulted in compromised social memory formation, i.e., the ability to remember a conspecific (Hitti and Siegelbaum, 2014; Stevenson and Caldwell, 2014). In rodents, this form of hippocampal-dependent memory profoundly relies on olfaction. CA2 PNs receive a strong connection from the entorhinal cortex (Chevaleyre and Siegelbaum, 2010), a structure that has been shown to be implicated in odor processing (Leitner et al., 2016) and to transmit sensory information to the hippocampus. Thus, there may exist a potential olfactory feedback connection between hippocampal area CA2 and the olfactory bulb, via CA1 RGCs, contributing to the processing of social olfactory information in the hippocampus. Our results have been obtained from dorsal hippocampus. However, both anatomical and functional studies have shown that dorsal CA2 PNs project to the ventral area CA1 (Meira et al., 2018; Tamamaki et al., 1988). Therefore, although more experiments have to be performed to conclude that CA2 transmission is similar in dorsal and ventral CA1, it is likely that our conclusion also applies to the ventral hippocampus.

STAR★METHODS

Detailed methods are provided in the online version of this paper and include the following:

- KEY RESOURCES TABLE
- CONTACT FOR REAGENT AND RESOURCE SHARING
- EXPERIMENTAL MODEL AND SUBJECT DETAILS
- METHOD DETAILS
  - Stereotaxic injection
  - Slice preparation
  - Electrophysiological recordings
  - Immunohistology and analysis
- QUANTIFICATION AND STATISTICAL ANALYSIS

SUPPLEMENTAL INFORMATION

Supplemental Information can be found online at https://doi.org/10.1016/j.celrep.2019.03.014.

ACKNOWLEDGMENTS

This work was funded by ATIP-Avenir program (to V.C.), ANR CA2-Gate (to V.C.), the Ville de Paris Programme Emergences (to R.A.P.), and the ANR Hippo-Hypo and ANR WhoRU (to R.A.P.). Confocal imaging was performed at the Université Paris Descartes FR3636 Service Commun de Microscopie and the IPNP imaging platform. Jonathan Bradley, Patrick Pierrot, Ali Jalil, Sandrine El Marhomy, and Cécile Violet provided valuable technical assistance.

AUTHOR CONTRIBUTIONS

Conceptualization, K.N., R.A.P., and V.C.; Investigation, K.N., V.R., and R.A.P.; Electrophysiological Recordings, V.C.; Immunohistology Experiments and Imaging, N.K., L.T., and R.A.P.; Cell Reconstruction and Quantification, L.T.; Writing – Original Draft, K.N., V.C., T.J.M., and R.A.P.; Writing – Review & Editing, V.C. and R.A.P.; Funding Acquisition, R.A.P. and V.C.; Resources, T.J.M.; CACNG5-cre Mouse Line and Viral Vectors, A.J.Y.H.

DECLARATION OF INTERESTS

The authors declare no competing interests.

Received: July 12, 2018
Revised: December 12, 2018
Accepted: March 2, 2019
Published: April 2, 2019

REFERENCES

Bannister, N.J., and Larkman, A.U. (1995). Dendritic morphology of CA1 pyramidal neurones from the rat hippocampus, I: branching patterns. J. Comp. Neurol. *360*, 150–160.

Boehringer, R., Polygalov, D., Huang, A.J.Y., Middleton, S.J., Robert, V., Wintzer, M.E., Piskorowski, R.A., Chevaleyre, V., and McHugh, T.J. (2017). Chronic loss of CA2 transmission leads to hippocampal hyperexcitability. Neuron *94*, 642–655.e9.

Botcher, N.A., Falck, J.E., Thomson, A.M., and Mercer, A. (2014). Distribution of interneurons in the CA2 region of the rat hippocampus. Front. Neuroanat. *8*, 104.

Bullis, J.B., Jones, T.D., and Poolos, N.P. (2007). Reversed somatodendritic I_h gradient in a class of rat hippocampal neurons with pyramidal morphology. J. Physiol. *579*, 431–443.

Buzsáki, G. (2015). Hippocampal sharp wave-ripple: a cognitive biomarker for episodic memory and planning. Hippocampus *25*, 1073–1188.

Chevaleyre, V., and Siegelbaum, S.A. (2010). Strong CA2 pyramidal neuron synapses define a powerful disynaptic cortico-hippocampal loop. Neuron *66*, 560–572.

Crépel, V., Khazipov, R., and Ben-Ari, Y. (1997). Blocking $GABA_A$ inhibition reveals AMPA- and NMDA-receptor-mediated polysynaptic responses in the CA1 region of the rat hippocampus. J. Neurophysiol. *77*, 2071–2082.

Erbs, E., Faget, L., Scherrer, G., Kessler, P., Hentsch, D., Vonesch, J.-L., Matifas, A., Kieffer, B.L., and Massotte, D. (2012). Distribution of delta opioid receptor-expressing neurons in the mouse hippocampus. Neuroscience *221*, 203–213.

Glickfeld, L.L., Atallah, B.V., and Scanziani, M. (2008). Complementary modulation of somatic inhibition by opioids and cannabinoids. J. Neurosci. *28*, 1824–1832.

Gulyás, A.I., Tóth, K., McBain, C.J., and Freund, T.F. (1998). *Stratum radiatum* giant cells: a type of principal cell in the rat hippocampus. Eur. J. Neurosci. *10*, 3813–3822.

Hitti, F.L., and Siegelbaum, S.A. (2014). The hippocampal CA2 region is essential for social memory. Nature *508*, 88–92.

Kay, K., Sosa, M., Chung, J.E., Karlsson, M.P., Larkin, M.C., and Frank, L.M. (2016). A hippocampal network for spatial coding during immobility and sleep. Nature *531*, 185–190.

Kirson, E.D., and Yaari, Y. (2000). Unique properties of NMDA receptors enhance synaptic excitation of radiatum giant cells in rat hippocampus. J. Neurosci. *20*, 4844–4854.

Klishin, A., Tsintsadze, T., Lozovaya, N., and Krishtal, O. (1995). Latent N-methyl-D-aspartate receptors in the recurrent excitatory pathway between hippocampal CA1 pyramidal neurons: $Ca(2^+)$-dependent activation by blocking A1 adenosine receptors. Proc. Natl. Acad. Sci. USA *92*, 12431–12435.

Knable, M.B., Barci, B.M., Webster, M.J., Meador-Woodruff, J., and Torrey, E.F.; Stanley Neuropathology Consortium (2004). Molecular abnormalities of the hippocampus in severe psychiatric illness: postmortem findings from the Stanley Neuropathology Consortium. Mol. Psychiatry *9*, 609–620, 544.

Kohara, K., Pignatelli, M., Rivest, A.J., Jung, H.-Y., Kitamura, T., Suh, J., Frank, D., Kajikawa, K., Mise, N., Obata, Y., et al. (2014). Cell type-specific genetic and optogenetic tools reveal hippocampal CA2 circuits. Nat. Neurosci. *17*, 269–279.

Lee, S.-H., Marchionni, I., Bezaire, M., Varga, C., Danielson, N., Lovett-Barron, M., Losonczy, A., and Soltesz, I. (2014). Parvalbumin-positive basket cells differentiate among hippocampal pyramidal cells. Neuron *82*, 1129–1144.

Leitner, F.C., Melzer, S., Lütcke, H., Pinna, R., Seeburg, P.H., Helmchen, F., and Monyer, H. (2016). Spatially segregated feedforward and feedback neurons support differential odor processing in the lateral entorhinal cortex. Nat. Neurosci. *19*, 935–944.

Leroy, F., Brann, D.H., Meira, T., and Siegelbaum, S.A. (2017). Input-timing-dependent plasticity in the hippocampal CA2 region and its potential role in social memory. Neuron *95*, 1089–1102.e5.

Mankin, E.A., Diehl, G.W., Sparks, F.T., Leutgeb, S., and Leutgeb, J.K. (2015). Hippocampal CA2 activity patterns change over time to a larger extent than between spatial contexts. Neuron *85*, 190–201.

Meira, T., Leroy, F., Buss, E.W., Oliva, A., Park, J., and Siegelbaum, S.A. (2018). A hippocampal circuit linking dorsal CA2 to ventral CA1 critical for social memory dynamics. Nat. Commun. *9*, 4163.

Mizuseki, K., Diba, K., Pastalkova, E., and Buzsáki, G. (2011). Hippocampal CA1 pyramidal cells form functionally distinct sublayers. Nat. Neurosci. *14*, 1174–1181.

Nasrallah, K., Piskorowski, R.A., and Chevaleyre, V. (2015). Inhibitory plasticity permits the recruitment of CA2 pyramidal neurons by $CA3^{1,2,3}$. eNeuro *2*.

Okuyama, T., Kitamura, T., Roy, D.S., Itohara, S., and Tonegawa, S. (2016). Ventral CA1 neurons store social memory. Science *353*, 1536–1541.

Oliva, A., Fernández-Ruiz, A., Buzsáki, G., and Berényi, A. (2016). Role of Hippocampal CA2 Region in Triggering Sharp-Wave Ripples. Neuron *91*, 1342–1355.

Pagani, J.H., Zhao, M., Cui, Z., Avram, S.K.W., Caruana, D.A., Dudek, S.M., and Young, W.S. (2015). Role of the vasopressin 1b receptor in rodent aggressive behavior and synaptic plasticity in hippocampal area CA2. Mol. Psychiatry *20*, 490–499.

Piskorowski, R.A., and Chevaleyre, V. (2013). Delta-opioid receptors mediate unique plasticity onto parvalbumin-expressing interneurons in area CA2 of the hippocampus. J. Neurosci. *33*, 14567–14578.

Piskorowski, R.A., Nasrallah, K., Diamantopoulou, A., Mukai, J., Hassan, S.I., Siegelbaum, S.A., Gogos, J.A., and Chevaleyre, V. (2016). Age-dependent specific changes in area CA2 of the hippocampus and social memory deficit in a mouse model of the 22q11.2 deletion syndrome. Neuron *89*, 163–176.

Senior, T.J., Huxter, J.R., Allen, K., O'Neill, J., and Csicsvari, J. (2008). Gamma oscillatory firing reveals distinct populations of pyramidal cells in the CA1 region of the hippocampus. J. Neurosci. *28*, 2274–2286.

Simons, S.B., Caruana, D.A., Zhao, M., and Dudek, S.M. (2011). Caffeine-induced synaptic potentiation in hippocampal CA2 neurons. Nat. Neurosci. *15*, 23–25.

Soltesz, I., and Losonczy, A. (2018). CA1 pyramidal cell diversity enabling parallel information processing in the hippocampus. Nat. Neurosci. *21*, 484–493.

Stevenson, E.L., and Caldwell, H.K. (2014). Lesions to the CA2 region of the hippocampus impair social memory in mice. Eur. J. Neurosci. *40*, 3294–3301.

Tamamaki, N., Abe, K., and Nojyo, Y. (1988). Three-dimensional analysis of the whole axonal arbors originating from single CA2 pyramidal neurons in the rat hippocampus with the aid of a computer graphic technique. Brain Res. *452*, 255–272.

Valero, M., Cid, E., Averkin, R.G., Aguilar, J., Sanchez-Aguilera, A., Viney, T.J., Gomez-Dominguez, D., Bellistri, E., and de la Prida, L.M. (2015). Determinants of different deep and superficial CA1 pyramidal cell dynamics during sharp-wave ripples. Nat. Neurosci. *18*, 1281–1290.

van Groen, T., and Wyss, J.M. (1990). Extrinsic projections from area CA1 of the rat hippocampus: olfactory, cortical, subcortical, and bilateral hippocampal formation projections. J. Comp. Neurol. *302*, 515–528.

Wintzer, M.E., Boehringer, R., Polygalov, D., and McHugh, T.J. (2014). The hippocampal CA2 ensemble is sensitive to contextual change. J. Neurosci. *34*, 3056–3066.

Zhao, M., Choi, Y.-S., Obrietan, K., and Dudek, S.M. (2007). Synaptic plasticity (and the lack thereof) in hippocampal CA2 neurons. J. Neurosci. *27*, 12025–12032.

STAR★METHODS

KEY RESOURCES TABLE

REAGENT or RESOURCE	SOURCE	IDENTIFIER
Antibodies		
Alexa 488 conjugated Goat α-Chicken	Life Technologies	A11039; RRID: AB_2534096; lot: 1812246
Chicken α-GFP	Abcam	Ab13970; RRID: AB_300798; lot: GR236651-10
Alexa 555 Goat α-Rat	Life Technologies	A21434; RRID: AB_2535855; lot:1670155
Rat α-mCherry	Life Technologies	M11217; RRID: AB_2536611; lot: QE214609
Rabbit anti-PCP4	Sigma	HPA005792; RRID: AB_1855086; lot: B97113
Rabbit anti-Glutamic Acid Decarboxylase 65/67	Sigma	G5163; RRID: AB_477019; lot: 101M4812
Alexa 555 Goat α-Rabbit	Life Technologies	A21428; RRID: AB_2535849; lot:1858260
Virus Strains		
AAV.DJ/8.hSyn.DIO.hM4D.Gi.mCherry	McHugh Lab	N/A
AAV9.EF1a.DIO.hChR2(H134R).EYFP	Penn Vector Core University of Pennsylvania School of Medicine	Addgene 20298
Chemicals, Peptides, and Recombinant Proteins		
AM251	TOCRIS	Cat#1117/1
Biocytin	Invitrogen	Cat#B1592
CGP55845 hydrochloride	HelloBio	Cat# HB0960
Clozapine N-oxide (CNO)	TOCRIS	Cat#4936
DAMGO	TOCRIS	Cat#1171/1
D-APV	TOCRIS	Cat#0106/1
DPDPE	TOCRIS	Cat#1431/1
Far-Red Nissl	Life Technologies	Cat#N21483
Naltrindole hydrochloride	TOCRIS	Cat#0740
SR95531 hydrobromide	HelloBio	Cat#HB0901
Streptavidin-conjugated Alexa 594	Life Technologies	Cat#S1125
Streptavidin-conjugated Alexa 647	Life Technologies	Cat#S21374
Experimental Models: Organisms/Strains		
Mouse: C57/B6J	Elevage Janvier	N/A
Mouse: cacng5-cre	McHugh Lab	N/A
Mouse: B6:129P2-Pvalbtm1(cre)ArbrlJ (Pvalb-cre)	The Jackson Laboratory	Cat#017320
Software		
Axograph X	Axograph	https://axograph.com/
Igor	Wavemetrics	https://www.wavemetrics.com/
ImageJ	ImageJ	https://imagej.net/Welcome
Neurolucida 360	MicroBrightField	https://www.mbfbioscience.com/neurolucida
Origin Pro	OriginLab	https://www.originlab.com/
pClamp10	Molecular Devices	https://www.moleculardevices.com/

CONTACT FOR REAGENT AND RESOURCE SHARING

Further information and requests for resources and reagents should be directed to and will be fulfilled by the Lead Contacts, Vivien Chevaleyre (vivien.chevaleyre@parisdescartes.fr).

EXPERIMENTAL MODEL AND SUBJECT DETAILS

6-12-weeks old male C57BL/6, cacng5-cre or Pvalb-cre mice were used for electrophysiological experiments. All animals were group housed in a standard 12 hr light/12 hr dark cycle and had free access to food and water. All procedures were approved and performed in accordance with the Université Paris Descartes Animal Experimentation ethical committee (ethic protocol number 2016040417305913-V10, Apafis #12406).

METHOD DETAILS

Stereotaxic injection

The adeno-associated viruses, AAV.DJ/8.hSyn.DIO.hM4D.Gi.mCherry, and AAV.EF1a.DIO.hChR2(H134R).EYFP were used at 3 × 108 vg. 500 nL of virus was injected bilaterally into the hippocampus of 6 - 8 week-old cacng5-cre or Pvalb-cre mice at 100 nL/min and the injection cannula was removed 5 minutes after infusion was complete. Injections were centered on: AP: −1.5 mm; ML: +/−1.8 mm; at a depth of 1.5 mm from the brain surface. The resulting infected area spanned at least 2 mm along the longitudinal axis of the hippocampus.

Slice preparation

400 μm transverse hippocampal slices were prepared two weeks following viral injection for the optogenetic experiments and 6 weeks following injection for Gi-DREADD experiments. From our previous work, we have not observed any differences in the synaptic transmission or properties of CA2 PNs between 6 and 30 weeks old animals. Animals were euthanized in accordance with institutional regulations with isofluorane and ketamine/xylazine anesthesia. Animals were intra-cardially perfused with oxygenated cutting solution containing (in mM): 93 NMDG, 2.5 KCl, 1.25 NaH2PO4, 30 NaHCO3, 20 HEPES, 25 Glucose, 2 thiourea, 5 Na-Ascorbate, 3 Na-pyruvate, 0.5 CaCl2, 10 MgCl2, 93 HCl. Hippocampi were removed and placed upright into an agar mold and cut with a vibratome (Leica VT1200S) in ice-cold solution and transferred to 30°C ACSF (in mM: 125 NaCl, 2.5 KCl, 10 glucose, 26 NaHCO3, 1.25 NaH2PO4, 2 Na Pyruvate, 2 CaCl2 and 1 MgCl2) for 30 min and maintained at room temperature for at least 1.5 hr prior to recording. For some experiments, a scalpel was used to make a small incision between CA2 and CA1 or between CA3 and CA2 under a dissection stereomicroscope immediately after cutting prior to incubation at 30°C. All experiments were performed at 33°C. Cutting and recording solutions were both saturated with 95% O2 and 5% CO2 (pH 7.4).

Electrophysiological recordings

Whole-cell recordings were obtained from hippocampal PNs in current clamp mode held at −78 mV with a patch pipette (3–5 MΩ) containing (in mM): 135 KMethylSulfate, 5 KCl, 0.1 EGTA-Na, 10 HEPES, 2 NaCl, 5 ATP, 0.4 GTP, 10 phosphocreatine and 5 μM biocytin (pH 7.2; 280–290 mOsm). Inhibitory currents were recorded with pipette solution containing 135 CsMethylSulfate instead of KMethylSulfate. When necessary, $GABA_A$ and $GABA_B$ receptors were blocked with 1 μM SR95531 and 2 μM CGP55845, respectively (HelloBio). The liquid junction potential was ∼8 mV and membrane potentials were corrected to account for this. Series resistance (typically 12–18 MΩ) was monitored throughout each experiment; cells with more than 15% change in series resistance were excluded from analysis.

Photostimulation with 0.1 ms pulses of blue light was achieved using a 473 nm light-emitting diode (controlled by a CoolLED model PE-100) driven by a TTL pulse. The light intensity used was between 10–50 mW/mm2. This was measured at the appropriate focal length under the objective with a Fieldmate model light meter (Coherent) at different power intensities. For extracellular recordings examining CA3-CA1 fEPSP, recording electrodes filled with 1 M NaCl were placed in SP of CA1. The stimulation electrode was placed 200 μm away from the CA2-CA1 border in CA1 SR. The stimulating pipettes were frequently moved to optimize evoked responses. GABA receptor blockers 1 μM SR95531 and 2 μM CGP55845 were bath-applied following dilution into the external solution from concentrated stock solutions. We used pClamp10 and Axograph X software for data acquisition. Axograph X, Igor and Origin Pro software was used for all data analysis.

Immunohistology and analysis

Recorded cells were filled with biocytin and post hoc labeling of filled cells with streptavidin-conjugated alexa-594 or alexa-647 was performed along with immunohistology to confirm cell identity. ChR2 was labeled with chicken α-GFP (Abcam) diluted 1:2000 with Alexa 488 conjugated goat α-chicken (Life Technologies) diluted 1:300. Gi-DREADD-mcherry was labeled with rat α-dsRed (Life Technologies) diluted 1:2000 and Cy3-goat α-rat. In order to assess if CA1 pyramidal cells were deep or superficial all neuronal soma were stained with a far-red or blue-conjugated nissl (Neurotrace, Life Technologies). Slices were mounted with ProLong Diamond (Thermofisher) and z series confocal images were collected with a Zeiss 710 LSM microscope. Image analysis was performed with ImageJ and cellular morphologies were reconstructed from confocal images with Neurolucida 360 (MicroBrightField).

QUANTIFICATION AND STATISTICAL ANALYSIS

Statistical analysis was performed using OriginPro software (OriginLab). We used Student's t tests and ANOVA when the data followed a normal distribution. When the distribution was not normal, we used non-parametric test (Wilcoxon and Man-Whitney tests, see Table S1). Statistical significance was set to $p < 0.05$ (*** indicates $p < 0.001$, ** indicates $p < 0.01$, and * indicates $p < 0.05$). All values are reported as the mean ± SEM.